Journal of Physics B: Atomic,
Molecular and Optical Physics

Excitation of the Ca atom from the metastable states by electron impact

To cite this article: I I Shafranyosh *et al* 1997 *J. Phys. B: At. Mol. Opt. Phys.* **30** 2261

J. Phys. B: At. Mol. Opt. Phys. **30** (1997) 2261–2285. Printed in the UK PII: S0953-4075(97)71272-0

Excitation of the Ca atom from the metastable states by electron impact

I I Shafranyosh†, T A Snegurskaya†, N A Margitich†, S P Bogacheva†, V I Lengyel† and O I Zatsarinny‡

† Uzhgorod State University, Department of Physics, Voloshina 32, Uzhgorod 294 000, Ukraine
‡ Institute of Electron Physics, Universitetska 21, Uzhgorod 294016, Ukraine

Received 23 January 1996, in final form 4 October 1996

Abstract. Electron impact excitation of the Ca atoms from the metastable $4s4p\,^3P_J$ states has been studied by an optical method in crossed atomic and electron beams in the energy range from threshold up to 30 eV. The relative excitation functions and the absolute values of the emission cross sections for 16 spectral transitions excited both from the metastable and ground states have been obtained. The experimental results are compared with the close-coupling and Born–Ochkur calculations carried out with the extensive many-configuration target wavefunctions. In most cases the theoretical excitation functions agree within the limits of experimental error (50%) with the experimental results including the resonance-like structure in the near-threshold region allowing us to classify uniquely the resonances observed.

1. Introduction

Elementary collisions with excited particles are of both applied and fundamental interest. Such processes determine to a considerable extent the energy balance for different plasma and laser devices, while the understanding of the mechanisms of these processes allows one to study comprehensively the properties of atomic systems and their structure. The processes of electron excitation from the metastable states are of special interest. Among the variety of excited atomic particles in plasma, the metastable ones play a specific role due to their large lifetimes (in some cases above 10^{-5} s). One should also expect that the corresponding cross sections will be large since the atomic shells of the excited states are much more expanded.

At the same time, there is a serious lack of both theoretical and experimental data on the stepwise excitation (i.e. the excitation from the excited states) of atoms and molecules by electron impact. This is due to the additional difficulties in performing the experiments with excited targets which are related to the production of the excited (metastable) particles of sufficiently large concentrations, the accurate determination of these concentrations, and the detection of a signal above the strong accompanying background. In turn, the lack of experimental data does not stimulate the development of adequate theoretical models for the electron interaction with the excited atoms. A comprehensive review of cross section measurements for electron impact on excited atomic species has been recently given by Trajmar and Nickel (1993). The previous measurements for atom excitation from the metastable states dealt primarily with the inert-gas atoms (see, e.g., Mityureva *et al* 1989, Johnson *et al* 1996 and relevant references therein). The works of Stumpf and Gallagher (1985) for Na as well as our early studies of the alkaline-earth atoms (Aleksakhin *et al*

1988, Shafranyosh *et al* 1990, 1994a, b) may also be mentioned. There are only a few relevant theoretical publications, for example, for the alkaline-earth atoms, the electron-impact excitation from the metastable states has only been studied by Peterkop and Liepinysh (1979), where the excitation cross sections for Cu and Sr were calculated using the Born–Ochkur method.

In the present work, we have developed an original experimental apparatus and a new method for studying the stepwise excitation of atoms that allowed us to obtain systematic data on the electron-impact excitation cross sections for the Ca atom in the metastable states. The data obtained include the 16 spectral transitions (ST) to various excited levels and give the basis for a further detailed study of the general regularities of electron interaction with atoms in the metastable states. For closer inspection of the cross sections obtained, extensive calculations within the framework of the close-coupling approximation have also been performed. Similar results for other alkaline-earth atoms will be published later.

2. Experimental technique and method

The present investigation of the stepwise excitation of the Ca atom from the metastable states was carried out by an optical method using crossed atomic and electron beams. The measurements were performed by means of an experimental set-up comprising a collision cell, an electron beam source and a system of radiation detection. The schematic layout of the set-up is shown in figure 1.

A five-electrode electron gun provided the following electron beam parameters: the beam current was 20 μA (at $E = 30$ eV) with an energy spread of 0.6 eV. Electron beam current was detected by the usual Faraday cup in the form of a 40 mm long hollow cylinder (kept at low positive potential with respect to the collision region to prevent secondary electrons from re-entering the collision region). In some special cases, for more precise measurements of resonance structure in the near-threshold energy region, a cylindrical 90° electron monochromator was used. This monochromator provided an electron beam of about 2 μA current within the 2–10 eV electron energy range at 0.2 eV energy spread. The electron beam was modulated by rectangular pulses of 720 Hz frequency and an on–off ratio of 1. The electron energy scale was calibrated against the excitation thresholds of the most intense spectral lines excited from the ground atomic states with an accuracy of 0.1 eV for the monochromated beam and 0.3 eV when the non-selected electron gun was used.

The metastable beam was produced by the discharge method (see figure 1). At the first stage, the ground-state atomic beam was produced by an effusion source (1) with a system of collimating slits, S_1–S_3. At the second stage, the beam entered the cell (2) where a system of electrodes (a tungsten cathode, a grid and an anode) generated the discharge. Here the ground-state atoms were converted with high efficiency into the excited states by the discharge electrons. The short-lived excited states decayed practically at the point of formation, while the ions produced in the discharge were removed from the cell by an electrostatic capacitor (3). Thus, on exit from the discharge area, the atomic beam contained mainly atoms of two forms: ground- and metastable-state atoms. Then the atomic beam was additionally collimated by a set of diaphragms, S_6, and directed into the region of interaction with the electron beam (5). The flag (4) served to shut the Ca beam on/off. The distance between the discharge chamber and the electron beam was about 35 mm. At the end of its path the atomic beam was condensed on the atom collector (8) producing with time a distinct trace (condensate). The linear dimensions of this condensate as well as the known distance from the electron beam allowed the cross section $\ell \times b$ of the atomic beam in the collision region to be determined (the dimension ℓ is shown in figure 1, while b is

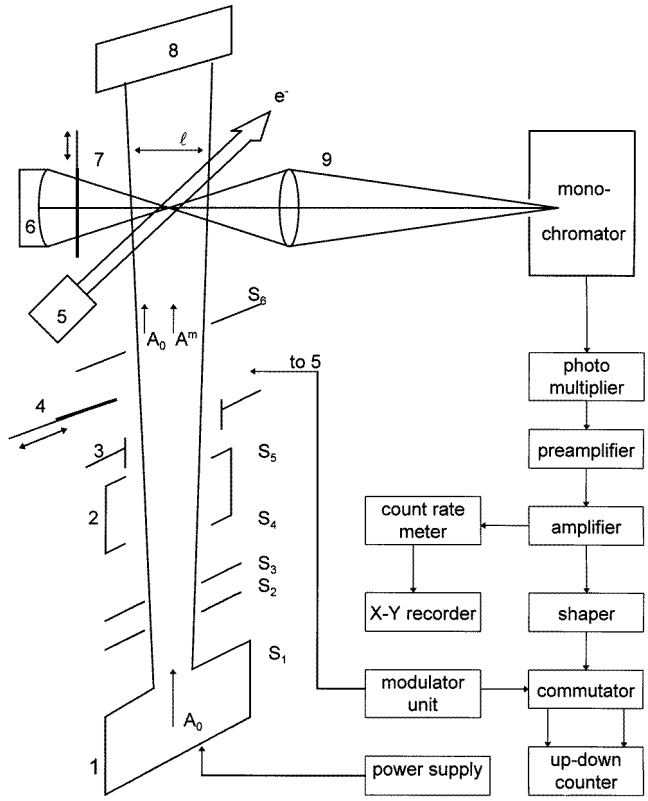

Figure 1. The experimental set-up and associated electronics. 1, effusion Ca atom source; 2, discharge chamber; 3, electrostatic capacitor; 4, atomic beam flag; 5, electron gun; 6, mirror; 7, mirror flag; 8, nitrogen trap; 9, lens; S_1–S_6, system of collimating slits.

the equivalent electron path inside the atomic beam).

The electron beam source and the metastable beam source were placed inside a stainless steel chamber with two quartz windows for extraction of the radiation. The vacuum in the chamber reached a base pressure of 10^{-7} Torr. The optical axis of observation was oriented normally to the electron and atomic beams. A 2 nm mm^{-1} linear reciprocal dispersion diffraction device with a 1200 lines/mm grating was used as an optical monochromator. The radiation detection system was operated in the separate photopulse counting mode under electron beam modulation.

The experiments on calcium atom excitation from the metastable states can be conditionally divided into three stages. In the first stage the emission spectrum for the Ca spectral lines was measured at 30 eV incident electron energy. The lines were identified by using the data of Moore (1949) and Striganov and Sventitsky (1966).

In the second stage the energy dependences of the excitation cross sections for the spectral lines were measured. The procedure for measuring the relative excitation functions for the spectral transitions under investigation was as follows: the radiation intensity of the given spectral line, $J(E)$, was twice separately measured as a function of the electron energy, E. First, when the atomic beam comprised atoms in both states, the dependence $J^m(E) + J^0(E)$ was measured, where $J^m(E)$ and $J^0(E)$ are the intensities of the spectral line related to the excitation of atoms from the metastable and ground states, respectively.

The second dependence, i.e. $J^0(E)$, was measured when the atomic beam comprised only the ground-state atoms. The difference between these two measurements, scaled by the electron beam current, I_e, defines the energy dependence of the excitation function, $Q^m(E)$, for the given spectral transition excited from the metastable states:

$$Q^m(E) = \frac{J^m(E) + J^0(E)}{I_e(E)} - \frac{J^0(E)}{I'_e(E)}, \tag{1}$$

where I_e is the electron beam current in the case when the Ca beam comprised two components (i.e. the metastable- and the ground-state atoms), I'_e is that for the case of a ground-state Ca beam. Note that the difference between I_e and I'_e did not exceed 5%. The experimental values of $(J^m + J^0)$, J^0, I_e and I'_e were computer-based processed to yield $Q^m(E)$.

In the third stage the absolute values of the excitation cross sections, Q^m, for the spectral lines under study were determined. In the optical method used by us, the following expression is the basic one to determine Q^m:

$$Q^m = I^m \lambda e / N^m j_e c d, \tag{2}$$

where I^m is the absolute intensity of the spectral line emission, λ is the wavelength, N^m is the metastable atom beam concentration in the region of its intersection by the electron beam, j_e is the electron beam density, d is the electron path inside the atom beam, e is the electron charge and c is the velocity of light. I^m and N^m are the most difficult quantities for experimental determination.

In the classical approach, the intensity, I^m, is conventionally derived by comparing it with the known intensity of a reference light source (a band lamp). Possessing a certain reliability, this approach, however, is quite laborious and complicated and, therefore, its application in our experiments with metastable atoms appeared to be problematic. Thus, we decided to choose another way where I^m is determined by comparing it with the intensity of the helium spectral line intensity, I^{He}, whose excitation cross section has already been measured with high accuracy (Van Zyl *et al* 1980).

The expression for the determination of Q^m obtained on the basis of equation (2) with allowance made for the relationship between the absolute and apparent intensities of the spectral line emission has a form:

$$\frac{Q^m}{Q^{He}} = \frac{J^m}{J^{He}} \frac{N^{He}}{N^m} \frac{K(\lambda_{He})}{K(\lambda_m)} \frac{\lambda_m}{\lambda_{He}} d/a. \tag{3}$$

Here the superscripts m and He denote the spectral lines under consideration and the He atom, J^m and J^{He} being the detected spectral line intensities, N^m and N^{He} being the concentrations of the corresponding atoms, and $K(\lambda_m)$ and $K(\lambda_{He})$ being the spectral sensitivities of the spectrophotometer at the given wavelength and a is the electron path inside the He atom medium specified by the distance between the accelerating electrode of the electron gun and a Faraday cup. Note that both J^m and J^{He} are measured at the same electron beam energy. It is seen from equation (3) that for all spectral lines Q^m values are strictly interlinked.

The quantities involved in equation (3) were evaluated as follows. At 30 eV electron energy the values J^m for the Ca spectral lines under study were measured and then the concentrations of the ground-state and metastable Ca atoms were determined (see below). Then the flag (figure 1, 4) was operated to cut off the Ca beam, the vacuum chamber was filled with helium up to 1×10^{-4} Torr, and J^{He} was measured at stable experimental conditions (similar to the measurements of J^m) for lines with 416.9, 443.8 and 504.8 nm wavelengths. To exclude the possible errors related to the definition of the d and a

parameters we have provided the experimental condition at which J^m and J^{He} were detected only from the central area of the beam intersection region. This was achieved by using two diaphragms—one rectangular (1×4 mm) mounted at the entrance slit of the monochromator and one round (20 mm diameter) placed at the lens. If one takes into account that the electron beam in the collision region is obviously narrower than the atomic beam, then one may assume correctly that $d/a = 1$. In parallel with the J^{He} measurements the total He ion current produced was recorded allowing one to define the helium atom concentration, N^{He}, by the known ionization cross section (Montaque *et al* 1984).

The correct solution of the problem of measuring the ion current is an important task and we have performed it in the following way. An ion detector in the form of a rectangular chamber with a molybdenum wire electrode (gauge) was placed close to the region of the collisions of the electron beam with the He atoms. The He ions produced in the collision region were extracted by the negative potential of the gauge. The ion collection efficiency was determined by the current of ion saturation which occurred at the gauge potential of -27 V. When determining the He atom concentration the electron beam energy was 100 eV. The method of ion detection has been described in more detail elsewhere (Shafranyosh and Margitich 1996).

After this the vacuum chamber was opened and two continuous spectrum sources (i.e. the 800.0–330.0 nm ribbon tungsten lamp and the 220.0–360.0 nm low-voltage hydrogen lamp) were mounted at the conditional point of atomic and electron beam crossing and the value of $K(\lambda)$ was defined for the 220–800 nm spectral region.

When discussing the Q^m data (see sections 4.1 and 4.3), the use of the ratio of the cross section Q^m to that for the excitation of the same spectral lines from the ground state, Q^0, appeared to be useful. Such a ratio with the inclusion of equation (2) has the form:

$$\frac{Q^m}{Q^0} = \frac{J^m}{J^0}\frac{N^0}{N^m}, \tag{4}$$

where N^0 is the ground Ca atom concentration.

Experimentally the determination of Q^m/Q^0 was reduced to the measurement of J^m, J^0 at 30 eV and determination of N^m and N^0. It is important to note that expression (4) allows one to estimate the correctness of the method used for determination of Q^m. Indeed, defining Q^m from equation (3) and Q^m/Q^0 from equation (4), one has a possibility of finding Q^0. Table 1 illustrates the agreement of our Q^0 data with those of Garga *et al* (1974) and Kuchenev and Smirnov (1995). As follows from table 1, for most of the spectral transitions

Table 1. Comparison of effective excitation cross sections for the Ca atom spectral transitions from the ground state.

		Cross section $Q^0_{30}(10^{-17}$ cm$^2)$		
	Transition	Our data	Garga *et al* (1974)[a]	Kuchenev and Smirnov (1995)[b]
1	$4s5s\,^3S_1$–$4s4p\,^3P_2$	0.45	0.48	0.44
2	$4s4d\,^3D_J$–$4s4p\,^3P_2$	0.18	0.12	0.49
3	$4p^2\,^3P_J$–$4s4p\,^3P_J$	0.24	0.014	0.16
4	$3d4p\,^3P_J$–$4s3d\,^3D_J$	0.12	0.1	0.47
5	$3d4p\,^3D_J$–$4s3d\,^3D_J$	0.28	0.2	0.96

[a] Narrow atomic and electron beams data.
[b] Ribbon atomic and electron beams data.

a satisfactory agreement of our data with those of other papers is seen. At the same time the substantial differences are observed for some transitions which are now difficult to explain.

Expression (4) is also useful for the following application. In those cases when the value of Q^0 is known with a high degree of reliability from the literature, Q^m can be found from equation (4). Thus, there is no need to use the more complicated formula (3).

The absorption method (Frish 1963) was used to determine the value of N^m, N^0 based on the known relation:

$$\int_0^\infty \chi(\nu)\,\mathrm{d}\nu = \frac{e}{m_0 c} f_{mk} N. \tag{5}$$

Here m_0, e are the electron mass and charge, respectively, c is the velocity of light and f_{mk} is the $m \to k$ transition oscillator strength, $\chi(\nu)$ is the absorption coefficient at the frequency ν, N is the absorbing atom concentration. If $\chi(\nu)$ is known, the integral in the left-hand side of (5) can be calculated numerically.

Let us present the absorption coefficient in the form $\chi(\nu) = \chi(0) f_\chi(\nu)$ and the intensity of the spectral line absorbed as $I(\nu) = I(0) f_I(\nu)$, where $\chi(0)$ and $I(0)$ are the absorption coefficient and the intensity in the central part of the line, respectively, $f_\chi(\nu)$ and $f_I(\nu)$ are the functions which define the frequency responses of the absorption coefficient and intensity, respectively. As is well known (Frish 1963), within the spectral line width, $\chi(\nu)$ is expressed by the same function of the frequency, ν, as the intensity distribution, $I(\nu)$, for similar cases of line broadening and low optical densities of the medium. This, in turn, means that for such conditions the analytical expressions for $f_\chi(\nu)$ and $f_I(\nu)$ are similar. For the atomic beam conditions the Doppler effect is the main factor defining the form of $f(\nu)$ (within the approximation sufficient for our problem). In this case the analytical expression for $f(\nu)$ is known from Minkowski and Bruck (1935).

On this basis, after integrating, we obtain in an explicit form the formula for the concentration, where $\chi(0)$ is unknown and found experimentally.

To determine $\chi(0)$ we used the well known modification of the absorption method (the so-called single-mirror method, (Frish 1970)), based on the self-absorption (reabsorption) directly in the light source and modified for the atomic beam conditions.

The atomic beam containing the normal and the metastable components was intersected across the whole width by the ribbon electron beam whose energy was enough to excite all the spectral lines. A uniform luminous body was produced in the intersection region in which the radiation self-absorption (reabsorption) may occur. The optical observation axis was chosen normal to the symmetry axes of the electron and atomic beams. A concave mirror (figure 1, 6) and a spectrophotometer were mounted at both sides of the optical axis. The relative intensities of the line with the mirror being shut on (J') and off (J) were measured. The reflection of the light by the mirror results in a radiation flux of intensity RJ (R is the reflective index of the mirror at the given wavelength which accounts for the double transmission of the light through the vacuum windows) falling onto the luminous body from the mirror side. Then the relative absorption is:

$$A = \frac{(J - JR) - J'}{IR} = \frac{(1 + R) - J'/J}{R}. \tag{6}$$

On the other hand, one can consider A as the function of the optical density of the absorbing medium, $\chi(\nu)\ell$, where ℓ is an absorbing layer thickness. Let us present the integral analytical expressions for J and J'. According to Frish (1963), J obeys the following expression:

$$J = \int_0^\infty \mathrm{d}\nu \frac{I(\nu)}{\chi(\nu)} \{1 - \exp[-\chi(\nu)\ell]\}. \tag{7}$$

Then

$$J' = J + R\int_0^\infty \mathrm{d}\nu \frac{I(\nu)}{\chi(\nu)}\{1 - \exp[-\chi(\nu)\ell\}\exp[-\chi(\nu)\ell]. \tag{8}$$

Using (7) and (8) we obtain the analytical expression for A:

$$A = 2 - \frac{\displaystyle\int_0^\infty \mathrm{d}\nu \frac{I(\nu)}{\chi(\nu)}\{1 - \exp[-2\chi(\nu)\ell]\}}{\displaystyle\int_0^\infty \mathrm{d}\nu \frac{I(\nu)}{\chi(\nu)}\{1 - \exp[-\chi(\nu)\ell]\}}, \tag{9}$$

the numerical integration of which defines the relationship between A and $\chi(0)\ell$. Thus, using the experimental value of A and the corresponding $\chi(0)$ we define the concentration of the absorbing atoms by formula (5). In the case of measuring A for those spectral lines whose lower level is the ground one we obtain the ground-state atom concentration, while in the case when the metastable level is the lower one the metastable atom concentration is obtained.

The He atom concentration was not determined by using the method described above since the resonant helium line (λ58.4 nm) lies in the vacuum UV region which is beyond the technical abilities of our experimental technique.

The concentrations of atoms in the ground and in the metastable states reached the values of 5×10^{10}–7×10^{10} cm^{-3} and 3×10^{9}–6×10^{9} cm^{-3}, respectively.

The relative error for the energy dependence of the cross sections was estimated to be not larger than 5% for strong ST and 8% for weak ST. The absolute excitation cross section uncertainty was about 50%. The main contribution to this error (equation (3)) is made by the metastable concentration uncertainty and the absolute radiation intensity error.

3. Calculations

The main difficulty in the theoretical investigations of the alkaline-earth atom excitation is the well known strong configuration mixing in the target wavefunctions. Since an adequate description of the atomic structure is the necessary input for an accurate scattering calculation, we use the configuration-interaction (CI) wavefunctions to represent the target states. To evaluate the excitation cross sections in the first approximation, we use the simple Born–Ochkur method. It allows one to incorporate the extensive many-configuration target wavefunctions without trouble and to quickly obtain the cross sections in the case where the use of more precise methods is problematic because of the necessity of including the large number of channels. The Born–Ochkur approximation was used mainly to calculate the excitation cross sections for highly excited levels and to estimate the cascade contributions. For a more detailed study of the excitations for some low-lying levels, we used the close-coupling method within two (2CC) and six (6CC) state approximations. The first approximation is closely related to the distorted wave approximation and was used to study the influence of the distorted atomic potential on the excitation cross sections. The second approximation was used to study the influence of the channel coupling.

3.1. Calculation of the target wavefunctions

Since we consider only the states with the outer-electron excitation, the CI method was applied in the frozen-core approximation. In this approximation, the complete wavefunction

of the atom is expanded over the basis wavefunctions in which only the orbitals of the outer electrons are changed

$$\Psi^{LS} = \sum_{i=\{nl,n,'l'\}} \mathrm{C}_i \Phi_i^{LS}(\mathrm{core}, nl, n'l'), \tag{10}$$

where the core has the closed-shell configuration $1s^2 2s^2 2p^6 3s^2 3p^6$. The task, thus, is reduced to the two-electron case. The set of one-particle orbitals, nl, used for the construction of the basis functions, Φ_i, was obtained from Hartree–Fock calculations of the $3p^6 nl$ states in the corresponding single-charged ion. In the present calculations, this set includes up to 50 orbitals with quantum numbers of $n \leqslant 14$, $l \leqslant 3$ and was not changed during the calculations. Such an application of the same orthogonal set of one-particle orbitals for various excited atomic states is very convenient in the cross section calculations in question.

The energy of the excited atomic states and corresponding expansion coefficient, C_i, were obtained by diagonalizing the complete nonrelativistic Hamiltonian on the basis which includes from 60 to 100 functions, and which is sufficient for stabilizing the lowest five to six states of each atomic Rydberg series under consideration. For each LS term, the set of the basic functions always includes the states with the $4snl$, $3\,dnl$, $4pnl$, $5snl$ configurations where nl runs over all values in the one-particle set indicated above, and some higher-lying configurations $nln'l'$ with comparable values of the nl and $n'l'$ numbers.

Using a sufficiently large set of the above basic wavefunctions, we can describe quite exactly the correlation between the outer electrons, but the correlation between the core and the valence electrons still remains beyond consideration. In the Ca atom, the core is many-electron, therefore, the correlation is expected to be important. To include the core–valence correlation, the wavefunction of the valence electron in the $3p^6 nl$ configuration was calculated with the modified core potential $V_{\mathrm{core}} = V_{\mathrm{HF}} + V_{\mathrm{pol}}$, where V_{HF} is the static Hartree–Fock potential, and V_{pol} is the model potential, which simulates the polarization of the core by the outer electron. V_{pol} and its parameters used in the present calculations are given in Zatsarinny *et al* (1989), where the influence of core polarization on the electron-impact excitation of Ca^+, Sr^+ and Ba^+ has been studied. The above procedure for the calculation of the level parameters and the wavefunctions in the case of alkaline-earth atoms has been described in more detail in our previous paper (Zatsarinny *et al* 1991).

Table 2 presents the binding energies for the triplet levels incorporated in the present scattering calculations and for some singlet levels for comparison. The energies obtained are compared with the most recent calculations by Mitroy (1993) carried out in terms of the CI method with the inclusion of a semi-empirical core-polarization potential (CIVP). Also given in table 2 are binding energies computed within the *ab initio* multi-configuration Hartree–Fock (MCHF) approach. For the present calculations, the largest discrepancy between the computed and experimental energies is 0.004 au. For the majority of levels, the difference between the theory and experiment is less than 0.001 au. The obtained accuracy is comparable with that of Mitroy (1993). The latter calculation is very similar to our calculation and differs only by a more sophisticated choice of the one-electron radial functions, which are not the same for all atomic states. As mentioned above, such choice of the radial orbitals is not convenient for scattering calculations. The comparison between the present CI calculations and those of Mitroy (1993) provides a test of the obtained CI expansions for the atomic wavefunctions used in the present scattering calculations. Comparison with the MCHF results (table 2) shows that the core-polarization potential must be included to achieve a good agreement between theory and experiment. The corresponding corrections vary from 0.02 to 0.04 au.

Table 2. Theoretical and experimental (Bashkin and Stoner 1975) binding energies (in atomic units) relative to the Ca^{2+} ionization limit for some low-lying states of neutral calcium. The experimental energies for triplets represent the mean of the fine structure levels. Present results are compared with the energies obtained by Mitroy (1993) in the CI method with the inclusion of a semi-empirical core-polarization potential, CIVP, and with the *ab initio* MCHF (Froese Fischer and Hansen 1985 and Vaeck *et al* 1991).

Level	Experiment	Present	CIVP	MCHF
$4s^2\,^1S$	−0.660 93	−0.657 77	−0.659 70	−0.663 29
$4s5s\,^1S$	−0.509 12	−0.507 87	−0.508 70	−0.487 92
$4s5s\,^3S$	−0.517 22	−0.516 87	−0.517 07	
$4s4p\,^1P^o$	−0.553 16	−0.552 01	−0.553 57	−0.528 77
$4s4p\,^3P^o$	−0.591 38	−0.589 27	−0.590 31	
$4s5p\,^1P^o$	−0.493 56	−0.492 91	−0.493 53	−0.471 72
$4s5p\,^3P^o$	−0.494 32	−0.493 50	−0.493 90	
$4s3d\,^1D$	−0.561 37	−0.556 45	−0.559 70	−0.529 63
$4s3d\,^3D$	−0.568 17	−0.564 06	−0.566 72	
$4s4d\,^1D$	−0.490 98	−0.489 39	−0.489 61	−0.466 60
$4s4d\,^3D$	−0.488 91	−0.487 95	−0.487 88	
$4p^2\,^3P$	−0.485 47	−0.484 61	−0.486 22	
$3d^2\,^3P$	−0.439 71	−0.436 65	−0.437 88	
$3d4p\,^3P^o$	−0.481 69	−0.479 46	−0.480 15	
$3d4p\,^3D^o$	−0.486 73	−0.485 09	−0.486 47	
$4s5f\,^1F^o$	−0.456 78	−0.456 38	−0.456 58	
$4s5f\,^3F^o$	−0.456 97	−0.456 72	−0.456 78	

Table 3. Comparison of calculated and experimental oscillator strengths for some selected transitions of the calcium spectrum. The CIVP and MCHF notations are the same as in table 1. Experimental data are cited from Mitroy (1993) (see detailed references and discussions therein).

Transition	Present	CIVP	MCHF	Experiment
$4s^2\,^1S$–$4s4p\,^1P^o$	1.74	1.82	1.95	(1.71–1.81) ± 0.03
$4s^2\,^1S$–$4s5p\,^1P^o$	0.0011	0.001 08	0.017 4	0.000 91 ± 0.0019
$4s^2\,^1S$–$4s6p\,^1P^o$	0.027	0.037 2	0.001 64	0.041 ± 0.006
$4s^2\,^1S$–$3d4p\,^1P^o$	0.055	0.072 7	0.007 98	0.066 ± 0.008
$4s^2\,^1S$–$4s7p\,^1P^o$	0.037	0.035 9	0.110	0.032 ± 0.004
$4s4p\,^1P$–$4s6s\,^1S$	0.0035	0.000 91	0.001 01	0.0090 ± 0.0006
$4s4p\,^1P$–$4p^2\,^1S$	0.116	0.120	0.149	0.114 ± 0.004
$4s4p\,^1P$–$4s7s\,^1S$	0.0136	0.016 4	0.016 5	0.0133 ± 0.0006
$4s4p\,^1P$–$4s4d\,^1D$	0.248	0.193	0.302	0.206 ± 0.005
$4s4p\,^1P$–$4p^2\,^1D$	0.497	0.550	0.465	0.579 ± 0.013
$4s4p\,^1P$–$4s5d\,^1D$	0.303	0.283		0.280 ± 0.006
$4s4p\,^1P$–$4s6d\,^1D$	0.063	0.052 8		0.0440 ± 0.0015
$4s4p\,^3P$–$4s5s\,^3S$	0.160	0.156		0.12 ± 0.02
$4s4p\,^3P$–$4p^2\,^3P$	0.503	0.529		0.522 ± 0.013
$4s4p\,^3P$–$4s4d\,^3D$	0.377	0.371		0.44 ± 0.07
$4s4p\,^3P$–$4s5d\,^3D$	0.112	0.112		0.12 ± 0.03

Another, and much more sensitive, test of the quality of the wavefunctions can be obtained by computing the optical oscillator strengths. This test is directly relevant to the scattering calculations, since the oscillator strengths provide a measure of the strength of the coupling between the channels. Table 3 compares the present absorption oscillator strengths for some selected levels with a number of experimental values and with the CIVP

and MCHF values, which correspond to the binding energies discussed above in table 2. The present values were obtained in the length form using the theoretical energies and a modified form of the dipole operator, which includes the core-polarization corrections (see, e.g., Zatsarinny *et al* 1991). On the whole, the agreement between the present oscillator strengths distribution and the experimental one is fairly good. As an example, consider the f values from the $4s^2\,{}^1S$ ground level. The present calculation correctly reproduces the trend in the f-value sequence, in particular, the zero in the sequence at the $4s5p\,{}^1P$ level. There is also close agreement with the CIVP results of Mitroy (1993), especially for the triplet states, which is important in our following scattering calculations. The agreement with the MCHF calculations is worse. This gives further evidence for the importance of core polarization corrections.

3.2. Scattering calculations

In the Born–Ochkur method, the excitation cross section for the transition from level 0 to level 1 is defined by the expression:

$$\sigma_{01} = \frac{8\pi}{k_0^2}\int_{q_1}^{q_2}\sum_{i,j} C_i C_j \sum_{\kappa}\left(\frac{a_\kappa}{q^3} + \frac{g_\kappa q}{k_0^2} + \frac{a_\kappa}{k_0^2 q}\right) \times (R_{01}^{\kappa})^2\,\mathrm{d}q \tag{11}$$

where $k_0^2 = 2E_0$, $k_1^2 = k_0^2 - 2\Delta_{01}$, $q_1 = k_0 - k_1$, $q_2 = k_0 + k_1$, and

$$R_{01}^{\kappa} = \int_0^{\infty} P_0(r)[j_\kappa(qr) - \delta_{\kappa 0}]P_1(r)\,\mathrm{d}r.$$

Here atomic units are used, E_0 being the incident electron energy, Δ_{01} being the excitation energy. $P_0(r)$ and $P_1(r)$ are the radial wavefunctions of the transition electron in the initial and final basis configurations i and j, respectively; $j(qr)$ is a spherical Bessel function. Coefficients a_κ and g_κ depend on the angular and spin momentum of the initial and final states and for the transitions between two-electron states they are presented, for example, by Vainshtein *et al* (1979).

The first term in equation (11) describes the direct-excitation cross section, while the second one takes into account exchange, and the third one results from the interference between these two terms. All the above components in (11) appeared to be important when calculating the cross sections in the energy range under consideration (from the threshold to 30 eV).

The close-coupling calculations were performed by the IMPACT code (Crees *et al* 1978). In this version of the close-coupling approximation, the total wavefunction of the 'atom + electron' system is adopted in the form

$$\Psi^{LS\pi} = \sum_i A\{\varphi(L_i, S_i) * F_i(r_i\varepsilon_i\lambda)\}^{LS\pi} + \sum_j c_j \Phi_j^{LS\pi}. \tag{12}$$

The first sum describes the free channels as being the vector-coupled antisymmetrized products of the N-electron functions $\varphi(L_i S_i)$ of the target atomic state with spin–orbital functions for the scattered electron with radial parts F_i, energy ε_i, and orbital momentum l_i. In practice, we cannot use the infinity expansion and only a few channels, depending on the task under consideration, are retained. In present calculations, we used two approximations.

In the first approximation, 2CC, the sum over the target states includes only two states, the initial ($4s^2\,{}^1S$ of $4s4p\,{}^3P$) and final states for the transition under study. This approximation is close to the distorted wave method and allows us to study the influence of the distorted atomic potential on the excitation cross sections. In addition, the coupling

between the initial and final states warrants the normalization of the cross sections, i.e. the conservation of the flux.

In the second approximation, 6CC, the sum over the target states in (12) includes six states: five lowest-lying states ($4s^2\,{}^1S$, $4s4p\,{}^{1,3}P$ and $4s3d\,{}^{1,3}D$) and the final state for the transition under study. Hence, in this approximation, all important couplings for the initial states ($4s^2\,{}^1S$ or $4s4p\,{}^3P$) considered in the present work are included. Besides, for all transitions from the $4s4p\,{}^3P$ level, the coupling between the initial and final states through the intermediate $4s3d\,{}^3D$ level ($4s4p\,{}^3P \to 4s3d\,{}^3D \to nln'l'\,{}^3L$) was found to be the most important. Hence, only the couplings of the final state to the higher-lying levels remain uninvolved. To do this in a systematic manner, one has to include a very large number of the target states and the calculations appear to be extremely cumbersome. On the other hand, the inclusion of separate levels only does not guarantee the improvement of the resulting cross sections.

The correlated-type bound channels, Φ_j, in (12) are the $(N+1)$-electron functions constructed from the target orbitals, P_{nl}, and have the form:

$$\Phi^{LS\pi} = A\{\varphi(L_i S_i) \times P_{nl}\}^{LS\pi}. \tag{13}$$

The sum over Φ_j must be included in expansion (12) due to the orthogonality constraints $\langle F_i | P_{nl} \rangle = 0$ imposed on the continuum orbitals to simplify the resulting formulae. This gives the minimum set of the correlated wavefunctions, Φ_j. On the other hand, the functions Φ_j also allow one to account for the virtual trap of scattering electrons in the unfilled atomic shell. As the present calculations show, the inclusion of the bound channels Φ_j in the close-coupling expansion (12) drastically changes the excitation cross section in the near-threshold energy range.

Applying a variational principle to expansion (12), one arrives at a system of linear integro-differential equations for the radial wavefunctions F_i. This system of equations is also coupled through the matrix equations involving the parameters c_j. Present calculations within the close-coupling method were carried out for all partial waves with $L \leqslant 15$ (with full inclusion of exchange for $L \leqslant 8$). The contributions of the partial cross sections with $L > 15$ were evaluated in the Bethe approximation. Note also, that the target wavefunctions $\varphi(L_i S_i)$ in (12) and (13) are the many-configuration functions in the form of expansion (10). This makes the electron scattering calculations prohibitively time consuming. For this reason, we restricted the expansion (10) by the terms with the expansion coefficients $C_i > 0.01$. This reduces the number of basis functions to 10–20 terms. The control calculation shows that the resulting change of the oscillator strengths does not exceed 10%. The same errors might be also expected for the cross section calculations. In addition, to take into account the core polarization by the scattered electron, the core polarization potential was also introduced in the close-coupling equations, with the same parameters as used in the bound-state calculations.

4. Results and discussion

4.1. General remarks

The spectral transitions studied are shown in the energy-level diagram in figure 2. The Ca atom has three metastable states: the $3d4s\,{}^1D_2$ state with excitation energy of 2.71 eV and two triplet states, $4s4p^3P_0$ and ${}^3P_2$, with excitation energies of 1.88 eV and 1.90 eV, respectively. In our experiments, the concentration of the ${}^3P$ states ($\sim 5 \times 10^9$ cm^{-3}) exceeded considerably that of the ${}^1D$ state ($\sim 10^8$ cm^{-3}). Therefore, one might expect that

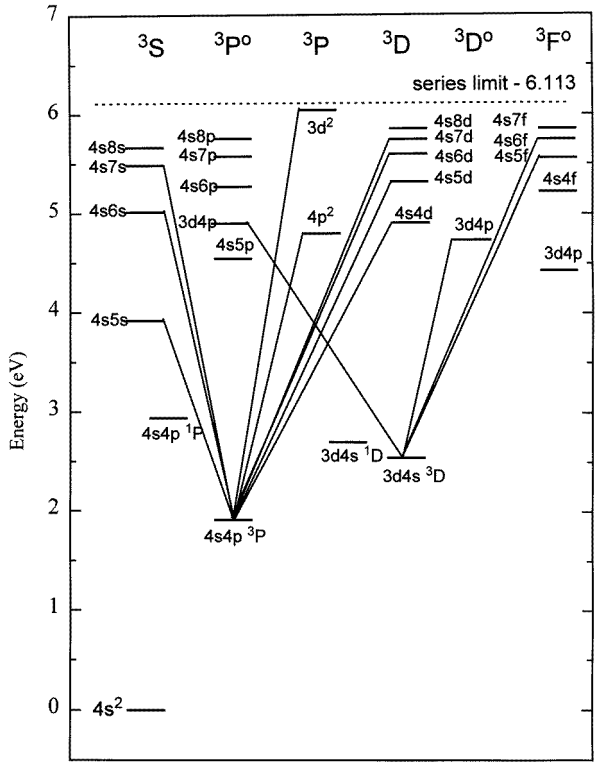

Figure 2. A simplified energy level diagram of Ca showing levels of interest. The arrowhead lines indicate the spectral transitions observed, the corresponding wavelengths are listed in table 4.

the contribution from the ^{1}D state to the total excitation from the metastable states is not essential. This is also supported by the measurements of the excitation thresholds. Table 4 presents the experimental values of the absolute cross sections for excitation of spectral lines in the Ca atom and their excitation thresholds, all of them being uniquely identified with excitation from the triplet metastable states 4s4p ^{3}P. Though a minor contribution from the singlet 3 ^{1}D state is also possible, it is assumed to lie within the limits of the relative radiative measurement error ($\sim$ 5%).

As follows from table 4, the largest values of the cross sections are observed for the first terms of the diffuse and sharp series (i.e. for the spectral transitions 4 ^{3}P–5 ^{3}S and 4 ^{3}P–4 ^{3}D) for which the excitation from the metastable states occurs with the minimum change of the principal quantum number. At 30 eV electron energy the absolute values of the stepwise excitation cross sections of spectral lines exceed considerably those for excitation from the ground states (see column Q^m/Q^0 in table 4). Such a large value of the parameter Q^m/Q^0 is mainly due to the fact that excitation of the spectral transition from the metastable states occurs predominantly in the process with the direct dipole interaction of the incident electron with the metastable atom, while these spectral lines are excited from the ground state only in the exchange interaction process accompanied by change of the atomic spin. The second terms of the diffuse and sharp series (i.e. the spectral transitions 4 ^{3}P–6 ^{3}S and 4 ^{3}P–5 ^{3}D) have essentially smaller cross sections as well as the parameter Q^m/Q^0. This circumstance seems to be important and indicates that the decrease of the cross sections

Table 4. Emission cross sections of the Ca atom spectral transitions excited from the metastable $4s4p\,^3P_J$ states. Cross sections are given in units of 10^{-17} cm^2, energies are given in eV, and the additional subscript of the cross sections Q specifies the electron energy. w_{if} denotes the branching ratio coefficient for the given transition.

No	Transition	λ (nm)	$E_{\text{threshold}}$	Q^m/Q^0_{30}	Q^m_{30}	Q^{BO}_{30}	$Q^{2\text{CC}}_{30}$	$Q^{6\text{CC}}_{30}$	w_{if}	Q^m/Q^0_{10}	$(Q^m/Q^0_{10})^{6\text{CC}}$
1	$4s5s\,^3S_1$–$4s4p\,^3P_2$	616.2	2.0	200	90	24.6	23.6	28.7	5/9	70.0	94.0
2	$4s5s\,^3S_1$–$4s4p\,^3P_1$	612.2	2.0	200	50	14.8	14.1	17.2	3/9		
3	$4s5s\,^3S_1$–$4s4p\,^3P_0$	610.2	2.0	200	20	4.9	4.7	5.7	1/9		
4	$4s7s\,^3S_1$–$4s4p\,^3P_J$	346.9–348.7	3.6	55	1.3	0.7			0.71		
5	$4s8s\,^3S_1$–$4s4p\,^3P_J$	326.9–328.6	3.8	25	0.3	0.3			0.69		
6	$4s4d\,^3D_J$–$4s4p\,^3P_2$	445.5–445.7	2.8	110	20	33.3	31.6	32.4	5/9	23.7	28.1
7	$4s4d\,^3D_J$–$4s4p\,^3P_{0,1}$	442.5–443.6	2.8	90	13.5	26.6	25.3	26.0	4/9		
8	$4s5d\,^3D_J$–$4s4p\,^3P_J$	362.4–364.5	3.4	140	12	12.2			0.86		
9	$4s6d\,^3D_J$–$4s4p\,^3P_J$	334.5–336.2	3.7	60	3.6	4.2			0.78		
10	$4s7d\,^3D_J$–$4s4p\,^3P_J$	321.0–322.6	3.9	30	1	2.2			0.68		
11	$4s5f\,^3F_J$–$4s3d\,^3P_J$	409.3–409.9	3.7	20	10	1.6	1.8	2.4	0.73	11.0	18.0
12	$4s6f\,^3F_J$–$4s3d\,^3D_J$	387.0–387.5	3.8	7	2	1.0			0.78		
13	$3d^2\,^3P_J$–$4s4p\,^3P_J$	299.5–300.9	4.1	180	14	7.4	6.2	5.7	0.61	20.5	115
14	$4p^2\,^3P_J$–$4s4p\,^3P_J$	428.3–431.8	2.9	230	56	131	91.9	91.1	1.0	145	250
15	$3d4p\,^3P_J$–$4s3d\,^3D_J$	526.0–527.0	3.0	60	7	1.5	1.6	3.5	1.0	5.4	4.0
16	$3d4p\,^3D_J$–$4s3d\,^3D_J$	558.2–560.3	2.9	95	27	2.3	2.0	4.6	1.0	14.1	8.3

within a given series appears to be more rapid for excitation from the metastable states than from the ground states. The evident exclusion from this rule is a spectral transition from the $5\,^3D$ level, for which an outstandingly large value of the parameter Q^m/Q^0 is observed.

Noticeable excitation of the spectral lines from the $4snp\,^3P^o$ levels as well as from the singlet levels was not observed experimentally which indicates the small value of the parameter Q^m/Q^0 for these transitions.

It is seen from table 4 that not only the spectral transitions from the normal levels, but also from the displaced levels with configurations $4p^2$, $3d^2$ and 3d4p are excited effectively and have the largest value of the parameter Q^m/Q^0. For example, the cross sections for the excitation of the $4s4p\,^3P$–$4p^2\,^3P$ transition exceed by approximately 230 times that excited from the ground state. In this regard it should be noted that the mechanisms of the excitation of the above spectral transitions from the ground and metastable states are of different nature. The excitation of the levels of the $4p^2$, $3d^2$ and 3d4p configurations from the ground state occurs due to the two-electron exchange transition ($4s^2$–$4p^2$ or $4s^2$–3d4p), whereas the excitation of these levels from the metastable state results from the one-electron dipole transtion (4s4p–$4p^2$ or 4s4p–3d4p).

The difference between the excitation mechanisms for the same spectral lines from the ground and metastable states is revealed not only in the magnitude but also in the shape of the energy dependence of the emission cross section. This is illustrated in figure 3, where the excitation functions from the metastable and ground states for seven spectral transitions are compared. It is seen that the energy behaviour of the cross sections for the excitation from the ground state (curve 1) possesses a near-threshold maximum with a rapid further decrease typical for the exchange interaction process. The energy behaviour of the cross section for the transitions excited from the metastable states (see figures 3(*a*)–(*c*), curve 2) has a completely different character: the maximum is reached at several threshold units indicating the important role of the process of dipole excitation. We assume that, just for this reason, the behaviour of curve 2 is similar to that of curve 3 (figure 3(*b*)) which

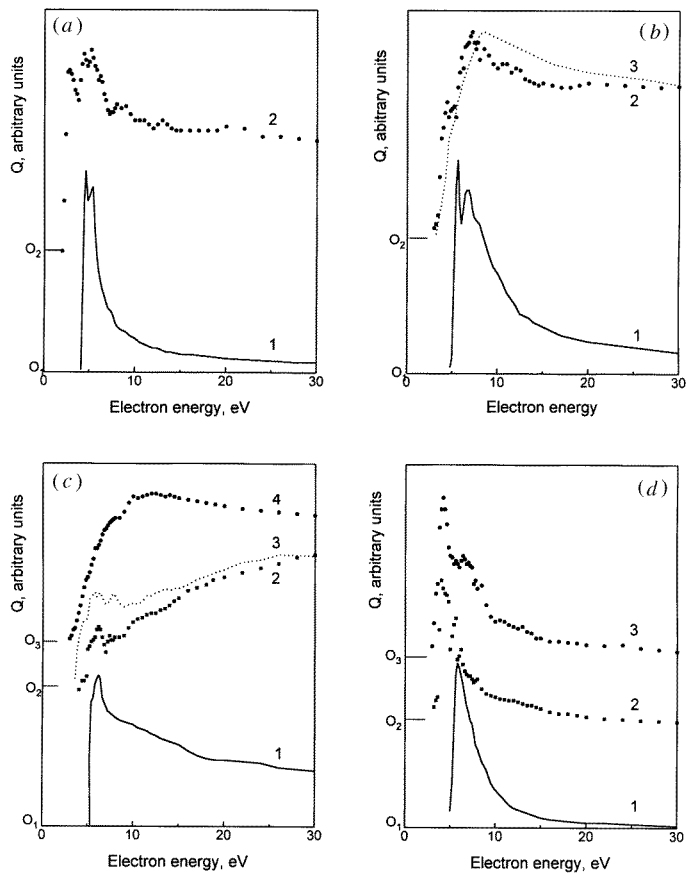

Figure 3. The excitation functions of the spectral transitions. (*a*) The $4s5s\,^3S_1 \rightarrow 4s4p\,^3P_J$ transition excited from the ground (curve 1) and metastable states (curve 2). (*b*) The $4s4d\,^3D_J \rightarrow 4s4p\,^3P_J$ transition excited from the ground (curve 1) and metastable states (curve 2) as compared with the $4s4p\,^1P_J$–$4s^2\,^1S$ spectral line (curve 3). (*c*) The $4p^2\,^3P_J \rightarrow 4s4p\,^3P_J$ transition excited from the ground (curve 1) and metastable states (curve 4) and the $3d^2\,^3P_J \rightarrow 4p4s\,^3P_J$ (curve 2), $4s5d\,^3D_J \rightarrow 4p4s\,^3P_J$ (curve 3) transitions excited from the metastable state. (*d*) The $3d4p\,^3P_J \rightarrow 4s3d\,^3D_J$ transition excited from the ground (curve 1) and metastable states (curve 2) and the $3d4p\,^3D_J \rightarrow 4s3d\,^3D_J$ (curve 3) transition excited from the metastable state.

corresponds to the excitation cross section of the resonant $4s^2\,^1S$–$4s4p\,^2P$ transition from the ground state.

Note the unusual character of the $3d^2\,^3P$ term excitation. The energy dependence of ST on this term (see figure 3(*c*), curve 2) is essentially similar to the excitation function for the $4s5d\,^3D$–$4s4p\,^3P$ transition (curve 3). This fact, as well as the proximity of the cross section for these different transitions, allows one to assume that the $3d^2\,^3P$ and $5\,^3D$ terms have the same additional mechanism of excitation from the metastable states, which suppresses the direct excitation.

Figure 3(*d*) shows the energy dependences of the excitation cross sections for ST emerging from the $3d4p\,^3D$, ^3P terms. As is seen, the curves corresponding to the excitation from the metastable states (curves 2 and 3) are similar both in general shape and structural peculiarities. At the same time, unlike the previous cases, no essential dissimilarity from

the curve related, say, to the excitation of the ^{3}P term from the ground state is seen (see figures 3(*a*)–(*c*)), though these terms are excited from the ground states only due to the exchange interaction. The physical explanation lies in that the displaced ^{3}P and ^{3}D terms are excited from the metastable states due to the quadrupole interaction, the value of which has the same order of magnitude as the exchange one. Besides, the shape of the quadrupole cross section is also usually characterized by the broad near-threshold maximum, just as in the case of the exchange transitions.

Thus, the above comparison of different cross sections for ST excited from the ground and metastable states shows that our experiment can serve as a direct tool for checking the influence of the exchange and dipole interactions on the energy dependences of the cross sections.

4.2. Theoretical results

The excitation cross sections calculated in three approximations (BO, 2CC and 6CC) are compared in figures 4–10. The calculations were carried out for seven triplet states excited from both the 4s4p ^{3}P metastable levels and ground state, and give the examples for different types of transitions, including direct dipole, monopole and quadrupole transitions as well as the exchange transitions, and two-electron ones. In this section, we discuss only the theoretical results, leaving the comparison with the experimental data to the next section.

First consider the strong dipole transitions 4s4p ^{3}P^o–4s5s ^{3}S, 4p^2 ^{3}P and 4s4d ^{3}D, presented in figures 4–6. For these transitions, all approximations agree closely with each other. This indicates that the dominant interaction in this case is a strong dipole interaction between the initial and final states, included in all approximations. Some difference is observed only in the near-threshold energy region and for the 4s4p ^{3}P^o–4p^2 ^{3}P transition where the BO cross section considerably exceeds the close-coupling results. This difference is most likely due to the well known unitarization effects which are more marked for transitions with large cross sections and with strong coupling to other scattering channels. A comparison between the BO and 2CC results shows that the own scattering channel unitarization is important only for the most strong 4s4p ^{3}P^o–4p^2 ^{3}P transition, whereas the comparison between the 2CC and 6CC results indicates that the coupling with the other scattering channels gives rise to the minor decrease of the near-threshold cross sections. Recall that the 6CC approximation includes all important couplings only for the initial state and additional inclusion of other strong couplings for the final state may result in a considerable decrease (as well as increase) of the near-threshold cross sections, but would only slightly affect the cross sections at higher energies. The above remark will be important in further comparisons of the absolute values of cross sections with experimental data.

In the case of the 4s4p ^{3}P^o–4s4d ^{3}D transition, depicted in figure 5, the close-coupling cross sections exhibit the pronounced resonance-like structure in the near-threshold energy region. The partial wave analysis shows that the first maximum is related to the (4s4d ^{3}D)εd resonances in the partial waves with $L = 1$–3. This structure becomes much less pronounced or dies away when the bound-type channels, Φ_j (equation (13)), are deleted from the total close-coupling expansion (12). We suggest that this resonance-like structure is due to the shape resonances and the necessary condition for their adequate description is the inclusion of the bound-type channels of equation (13) in the total close-coupling expansion (12). However, there is no direct one-to-one correspondence between Φ_j and the cross section resonances. First, the number of bound channels (up to the 20 terms) is much greater than the number of resonances revealed. Second, their energies never coincide with the resonance position. Thirdly, the influence of the bound channels on the cross section is much wider:

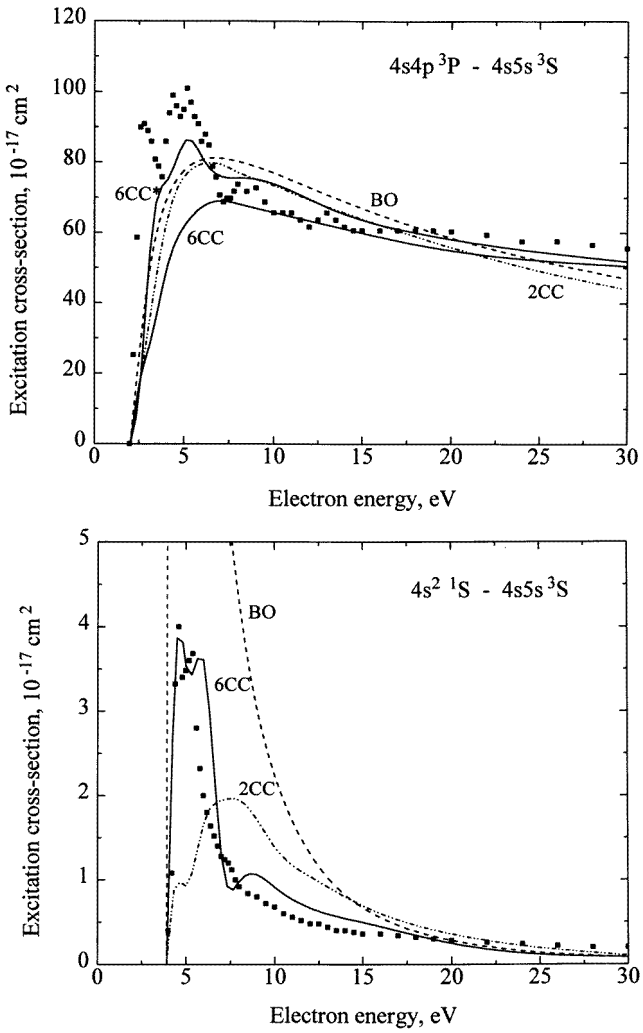

Figure 4. Comparison of the experimental excitation function with the close-coupling and Born–Ochkur calculations for the 4s5s ^{3}S–4s4p ^{3}P^o spectral transition excited from the metastable (upper figure) and ground (lower figure) states of Ca; theoretical data are presented on the absolute scale while the experimental results are plotted in accordance with the most general fit to the calculated data. •, experimental data; ——, 6CC results; — · · —, 2CC results; – – –, BO results. In addition, 6CC* denotes the 6CC results with the inclusion of the cascade contribution from the 4s5p ^{3}P^o level.

they give rise not only to the additional resonance structure, but also to the considerable increase of the cross section in a wide energy range from the threshold up to 15 eV. Thus, we can conclude that the resonances found are not related directly to Φ_j and result from a more adequate description of the scattering wavefunction and atomic potential due to the bound-type channels.

The influence of the bound channels is much more pronounced for weak transitions. Consider the example of the 4s4p ^{3}P^o–3d^2 ^{3}P dipole transition depicted in figure 7. The relatively large cross section for this two-electron transition is due to the strong configuration

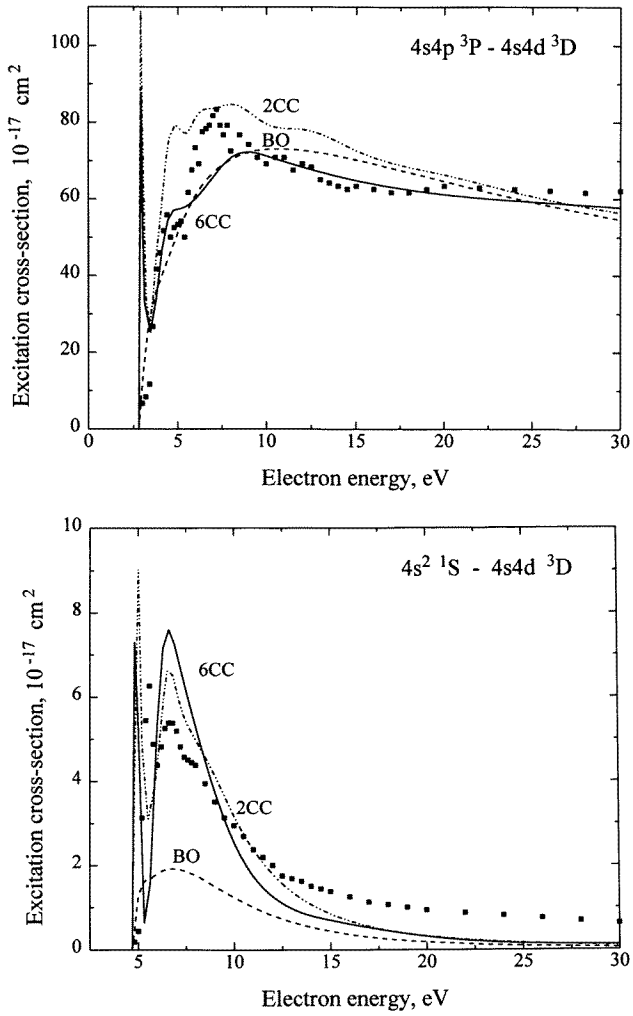

Figure 5. Same as in figure 4 for the 4s4d ^{3}D–4s4p ^{3}P^o transition.

mixing with the 4p^2 configuration. The BO cross section exceeds considerably the 2CC one, which, in turn, exceeds the 6CC results. This indicates the large unitarization effects for such transitions. The 2CC cross section displays two shape resonances in the ^{2}D and ^{4}D^o partial waves. In the 6CC approximation the first resonance is not seen and the second has much smaller intensity. It is a common feature for all resonances obtained: that the inclusion of additional couplings smooths out the resonance structure. To show the influence of the bound channels, the 6CC* cross section obtained with the exclusion of Φ_j from the close-coupling expansion is also presented in figure 7. We see that the inclusion of the bound channels leads to a considerable increase of the total cross section in a wide energy range from threshold to 15 eV.

The example of the monopole transition to the displaced level 3d4p ^{4}P^o is given in figure 8. In contrast to the dipole case, the 2CC results here exceed considerably the BO cross section in the near-threshold energy due to the influence of the bound channels and

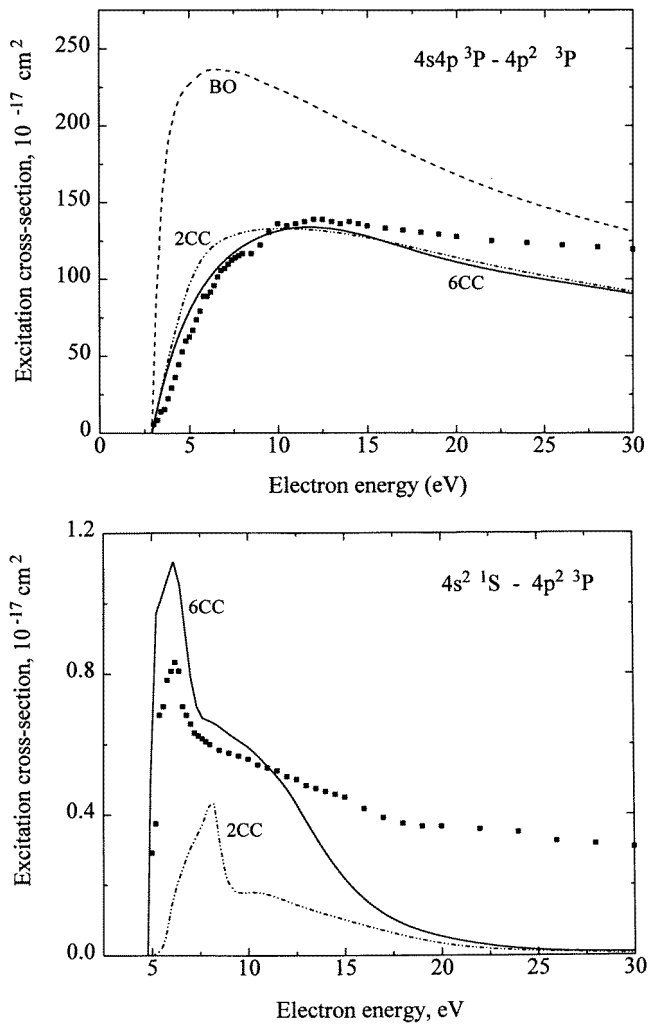

Figure 6. Same as in figure 4 for the $4p^2\,^3P$–$4s4p\,^3P^o$ transition.

agree well at the energies above 20 eV. In turn, the 6CC cross section exceeds considerably the 2CC results for all energies. This results from the large contribution of two-step virtual transitions via the intermediate state taken into account in the 6CC approximation. It was found that the most important coupling in this respect is the $4s4p\,^3P$–$4s3d\,^3D$–$3d4p\,^3P^o$ coupling. The resonance structure is almost fully smoothed out in the 6CC approximation and the main maximum at 5 eV is due to the large enhancement in the $^2P^o$ partial cross section.

The quadrupole $4s4p\,^3P^o$–$3d4p\,^4D^o$ and $4s4p\,^3P^o$–$4s5f\,^3F^o$ transitions presented in figures 9 and 10 show cross section behaviour similar to the monopole case discussed above. The main maximum in the first transition is due to the ^4D partial wave.

Turn now to the exchange excitations from the ground state. The values of the cross section are much smaller and affected strongly by the effects discussed above. Comparison of the BO cross sections with the close-coupling results shows that the BO approximation is not suitable in the low-energy region, even as a rough estimation. For example, the BO

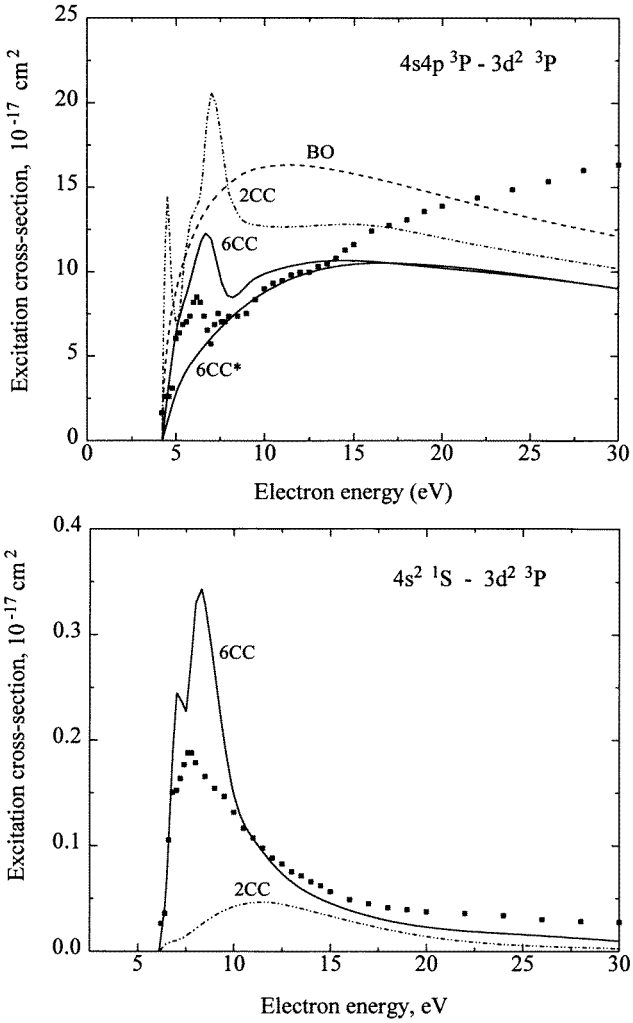

Figure 7. Same as in figure 4 for the 3d^2 ^{3}P–4s4p ^{3}P^o transition. In addition, 6CC* denotes the 6CC results without the inclusion of bound channels.

cross section for the monopole 4s^2–4s5s ^{3}S transition exceeds the CC results by an order in the main maximum, whereas for the multipole 4s^2–4s4d ^{3}D and 4s^2–4s5f ^{4}F transitions they are much smaller than the CC ones. The BO cross sections agree well with the CC ones only for the energies above 20 eV, but in this case the cross section is very small and is of no interest. For the two-electron transitions to the 4p^2, 3d^2 and 3d4p levels, the BO cross section is equal to zero due to the angular symmetry.

Almost for all exchange transitions considered, the 6CC cross sections exceed considerably the 2CC results, which indicates the large contribution of the two-step excitation via the intermediate level, mainly the 4s4p ^{1}P and ^{3}P levels (for example, 4s^2–4s4p ^{3}P–4s5s ^{3}S or 4s^2–4s4p ^{1}P–4s5s ^{3}S). The influence of the bound channels on the exchange cross sections is also very strong and results in the resonance structure and large near-threshold cross sections.

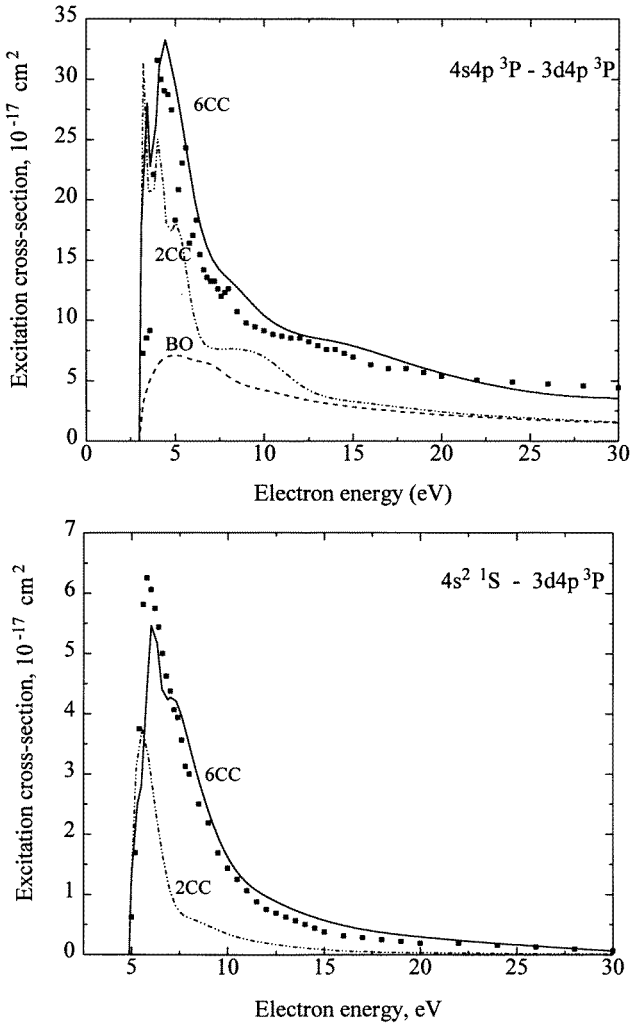

Figure 8. Same as in figure 4 for the 3d4p ^{3}P^o excitation.

4.3. Comparison of experimental and theoretical results

Comparison of the absolute emission cross section values is given in table 4, whereas the relative excitation functions are compared in figures 4–10. The emission cross sections differ from the excitation ones by the branching ratio coefficients and cascade contributions. The corresponding branching ratio coefficients were calculated using the theoretical decay probabilities and are also presented in table 4. For the spectral lines with the specified total orbital momentum, these coefficients also include the corresponding statistical factor. The cascade contribution was estimated from the BO calculations and turned out to be negligible at the electron energy of 30 eV and is not included in the theoretical emission cross sections.

As follows from table 4, for the most part of ST a reasonable agreement between the calculated and experimental absolute values is observed (within the limits of experimental error). At the same time for some ST (for example, emerging from the 4s5s ^{3}S$_1$, 4s5f ^{3}F$_J$, 3d4p ^{3}D$_J$ levels) one may notice a certain discrepancy between the experimental and

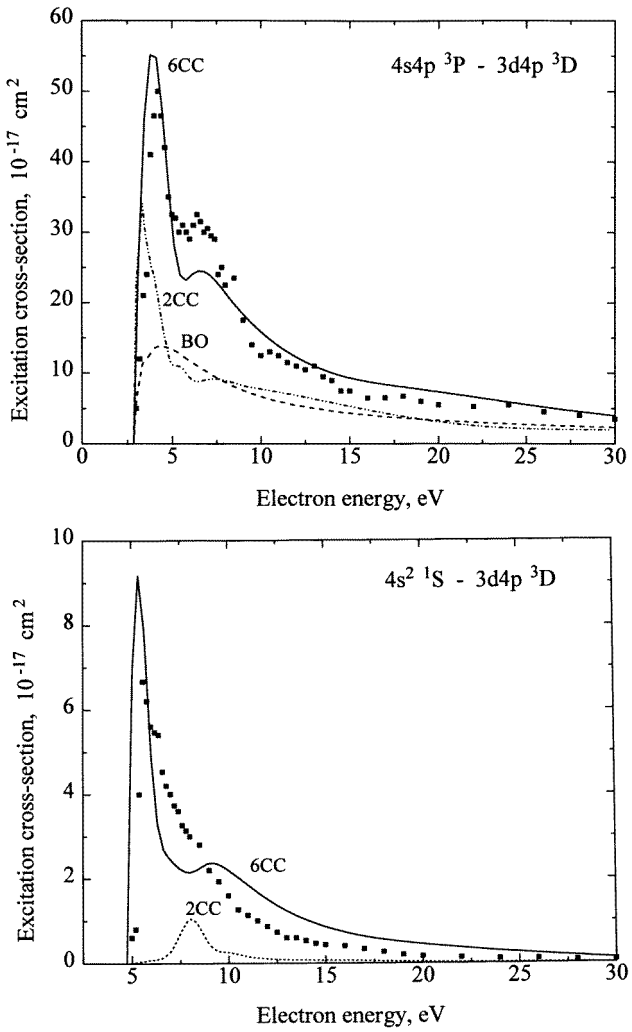

Figure 9. Same as in figure 4 for the 3d4p ^{3}D^o excitation.

theoretical data. The cause of this discrepancy is not obvious. Indeed, this disagreement lies beyond the experimental uncertainty and can hardly be explained by the systematic errors.

In the case of spectral transitions excited due to the monopole or quadrupole interaction, the most striking disagreement of the calculated and experimental cross sections is observed for two transitions: 4s4p ^{3}P–4s5f ^{3}F and 4s4p ^{4}P–3d4p ^{3}D. The theoretical values here cannot be considered as accurate as in the case of the dipole excitation because of the strong dependence on the approximation used. As discussed in the previous section, the inclusion of additional terms in the close-coupling expansion may lead to a considerable change of cross sections over a wide range of electron energies. Nevertheless, as is seen from table 4, the 6CC results agree with the experimental data much better than other approximations.

Our attention now turns to the exchange transitions from the ground state. Table 4 contains the ratio of the emission cross sections, Q^m/Q^0_{30}, for the spectral lines excited

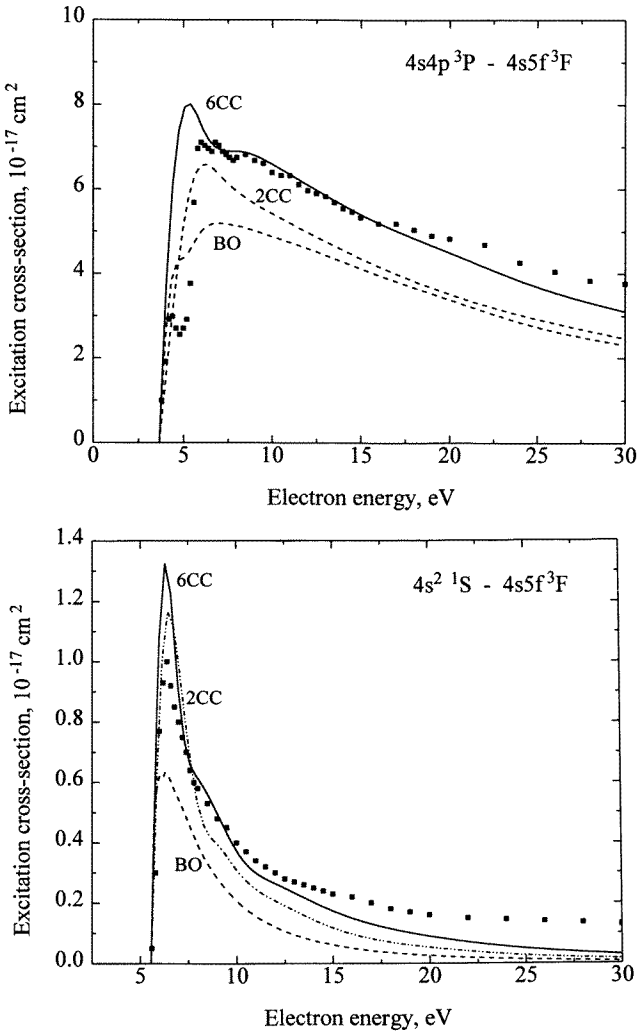

Figure 10. Same as in figure 4 for the 4s5f ^{3}F^o excitation.

from the metastable and ground states. These values were used to obtain the absolute normalization of the Q^m cross sections by known Q^0 according to formula (3). The above ratios are relatively large and reflect the large efficiency of direct excitation as compared with exchange excitation, however, the corresponding theoretical values are much larger. In this respect it is important to note that since the exchange cross sections are very small, the cascade contribution or other factors (for example, the spin–orbit interaction) may drastically change their magnitude. For the Ca atom, the spin–orbit interaction is relatively small but it is sufficient to affect strongly the exchange cross sections at higher energies. In the pure LS-coupling, the asymptotic behaviour of the exchange cross sections must be governed by the $1/E^3$ energy dependence. As is seen from figures 4–10, a large departure of most of the measured cross sections from the LS asymptotic is indirect evidence for the great influence of the spin–orbit interaction. We used the pure LS-coupled wavefunctions and due to the spin–orbit mixing the comparison of the experimental and theoretical ratios Q^m/Q^0 at 30 eV

is meaningless. Therefore, we chose the electron energy of 10 eV for such comparison and the corresponding quantities are presented in table 4. At this energy the exchange cross sections are large enough to ignore the spin–orbit mixing and, besides, there is no resonance structure which can be very sensitive to the approximation used. We see that the agreement between the experimental and theoretical ratios, Q^m/Q^0, is much better than for the absolute values of Q^m. Except for the $4p^2$ and $3d^2$ states, where the exchange cross sections are very small and spin–orbit mixing is sufficiently large to have a strong effect at all energies, the experimental and theoretical ratios Q^m/Q^0 agree within 50% for all transitions.

Turn now to the relative dependence of the excitation cross sections obtained. The accuracy achieved here (5%) is much higher than that for the absolute measurements. To facilitate the comparison of the energy dependence of the excitation cross sections obtained, the theoretical data in figures 4–10 are presented on an absolute scale while the experimental cross sections are normalized to fit to the calculated data.

In contrast to the calculations, the experimental $4s5s\,^3S$–$4s4p\,^3P$ emission cross section exhibits resonance-like structure in the near-threshold region. One of the possible reasons may be the cascade contribution. The 6CC* curve in figure 4 is the 6CC excitation cross section with the cascade contribution from the $4s5p\,^3P$ level calculated also in the 6CC approximation (note that the BO approximation gives a much smaller contribution). The $4s5p\,^3P$ state has a large branching ratio coefficient at the $4s5s\,^3S$ level (0.41) and gives the main part of the total cascade contribution. As is seen from figure 4, the second broad maximum can be related to the cascade from the $4snp\,^3P$ states. The first resonance cannot be related to any cascade contribution due to its energy position (see figure 2) and one may assume that this is the shape resonance not reproduced by the present 6CC calculations. The shape of the $4s^2$–$4s5s\,^3S$ exchange cross section is closely approximated by the 6CC results and differs considerably from the 2CC curve. This indicates that the main maximum is fully determined by coupling with other scattering channels.

In the case of the $4s4p\,^3P$–$4s4d\,^3D$ transition, figure 5, the close-coupling calculations predict the sharp shape resonance at the threshold not observed experimentally, probably due to the lack of the energy resolution. The broad maximum at 6–7 eV may also be attributed to the cascade contribution from the $4snp\,^3P$ levels. In the case of excitation from the ground state, the close-coupling calculations reproduce well the two-maxima form, the first maximum being the shape resonance.

For the $4s4p\,^3P^o$–$4p^2\,^3P$ transition (figure 6) the 6CC excitation function agrees well with the experimental results for low energies from the threshold to 15 eV. At higher energies the experimental curve begins to exceed progressively the close-coupling results. We believe that this may result from the contribution of some other scattering processes. The exchange $4s^2$–$4p^2\,^3P$ excitation function differs radically from the 6CC excitation function. The 6CC calculations reproduce correctly only the position of the main maximum. Large differences at high energies may be due to the extremely strong influence of spin–orbit mixing, especially with the $4p^2\,^1D$. According to the measurements of Kuchenev and Smirnov (1995), the $4s^3$–$4p^2\,^1D$ cross section has the magnitude of about $20–30 \times 10^{-17}$ cm^2 and smoothly decreases with energy. The contribution of a small part of this cross section due to the spin–orbit mixing may drastically change the $4s^2$–$4p^2\,^3P$ excitation function.

The experimental excitation function for the $4s4p\,^3P$–$3d^2\,^3P$ transition (figure 7) has an extraordinary form. Due to the energy position of the $3d^2\,^3P$ level close to the ionization limit, the cascade contribution is impossible here, and in analogy with the above case of the $4p^2$ excitation the additional scattering processes must be included into consideration to explain the energy dependence obtained. The 6CC calculations predict the shape resonance at energies of about 7 eV, which agree with the measurements. The 6CC calculations also

correctly predict the position of the main maximum for the exchange excitation of the $3d^2\,{}^3P$ level from the ground state, but the 6CC excitation function has more sharp shape than the experimental one.

For the $3d4p\,{}^3P$ displaced state, figure 8, the 6CC excitation function is in close agreement with the experimental data both for the direct excitation from the metastable level and the exchange excitation from the ground state. As is seen from the comparison of the 2CC and 6CC results, the necessary condition here is the inclusion of additional couplings with the $3d4s\,{}^{1,3}D$ and $4s4p\,{}^{1,3}P$ states for the direct and exchange excitation, respectively. Similar results were obtained for the excitation of another displaced term, $3d4p\,{}^3D$, figure 9. In addition, the 6CC calculations also confirm the double-peaked shape of the excitation function from the metastable state.

Finally, close agreement between the theoretical and experimental excitation functions was obtained for the $4s5f\,{}^3F$ level, figure 10. There is no resonance structure here and some high run of experimental excitation function can be attributed to the spin–orbit mixing effects.

As a whole, for most of the relative excitation function presented, a reasonable agreement with the 6CC calculations was obtained, including the resonance-like structure in the near-threshold region. Except for the case of strong dipole transitions, the 6CC results drastically differ from the less elaborate BO and 2CC approximations, and for the satisfactory agreement with the experimental results of the additional couplings with the $3d4s\,{}^{1,3}D$ and $4s4p\,{}^{1,3}P$ states is the necessary condition.

5. Summary and conclusions

We have reported the first measurements of the emission cross sections for a variety of electron-impact-induced transitions in the Ca atom excited from the $4s4p\,{}^3P^o$ metastable states. The results obtained are compared with the cross sections for the same spectral transitions excited from the ground state and with the extensive close-coupling calculations. The cross sections for some spectral transitions excited from the metastable states reach the value up to 10^{-15} cm^2 and exceed by two orders those excited from the ground state. For some transitions the resonance-like structure is observed in the near-threshold region. According to our close-coupling calculations, this structure is due to the shape resonances and is more pronounced for excitation from the metastable states. This effect is most revealed for the displaced states where the excitation cross sections from the ground states are also large and display the complicated structure. Such behaviour for the two-electron transitions directly indicates the importance of the correlation effects related to the strong configuration mixing in the alkaline-earth atoms. The relatively large cross sections for some exchange excitations at higher energies indicate also the large spin–orbit mixing in calcium.

Comparisons of various calculations show that the Born–Ochkur approximation gives reliable results only for strong dipole transitions, whereas for quadrupole or exchange transitions these calculations agree with the close-coupling data only above 25 eV. In most cases the 2CC calculations agree closely with the 6CC calculations, including the resonance structure in the near-threshold region. This confirms the assumption that the resonance structure is due to the shape resonances. Note that the inclusion of additional coupling smooths the resonance structure. Another strong influence on the cross sections results from the additional couplings with other scattering channels. For example, this causes the large increase of the quadrupole cross sections due to the virtual two-step transitions via the intermediate levels. The most important coupling was found to be that with the $3d4s\,{}^3D$

level for the quadrupole and monopole transitions from the ground state. The cascade contribution was found to be important only for excitation of the 4s*n*s ^{3}S and 4s4d ^{3}D levels, due to the strong near-threshold excitation of the 4s5p ^{3}P levels and results in a broad additional maximum at 6–10 eV energies.

Except for two transitions to the 4s5s ^{3}S and 3d4p ^{3}D levels, the absolute values of measured emission cross sections agree within the experimental error (50%) with the most elaborate close-coupling calculations. In this respect it seems very desirable to fulfil further independent measurements or calculations. There is no doubt that more detailed calculation or measurement will reveal rich resonance structure of cross sections.

Acknowledgments

The present study was supported in part by the International Soros Science Education Programme of the International Renaissance Foundation, grant SPU042037.

References

Aleksakhin I S, Nebesny F I, Semenyuk Ja I, Snegurskaya T A and Shafranyosh I I 1988 *Opt. Spektrosk.* **64** 431 (in Russian)
Bashkin S and Stoner J O 1975 *Atomic Energy Levels and Grotrian Diagrams* vol 2 (Amsterdam: North-Holland)
Crees M A, Seaton M J and Wilson P M H 1978 *Comput. Phys. Commun.* **15** 23
Frish S E 1963 *Optical Spectra of Atoms* (Moscow: Fizmatizdat) (in Russian)
—— 1970 *Spectroscopy of Gas Discharge Plasma* ed S E Frish (Moscow: Nauka) (in Russian)
Froese Fischer C and Hansen J E 1985 *J. Phys. B: At. Mol. Phys.* **18** 4031
Garga I I, Aleksakhin I S and Starodub V P 1974 *Opt. Spektrosk.* **37** 843–9 (in Russian)
Johnson M, Fujii K, Nickel J and Trajmar S 1996 *J. Phys. B: At. Mol. Opt. Phys.* **29** 531
Kuchenev S N and Smirnov Yu M 1995 *Phys. Rev.* **51** 578
Minkowski R and Bruck H 1935 *Z. Phys.* **95** 274
Mitroy J 1993 *J. Phys. B: At. Mol. Opt. Phys.* **26** 3703
Mityureva A A, Penkin N P and Smirnov V V 1989 *Opt. Spectrosc.* **67** 461
Montaque R G, Harrison M F H and Smith A C H 1984 *J. Phys. B: At. Mol. Phys.* **17** 3295
Moore C E 1949 *Atomic Energy Levels* (NBS Circular No 467) (Washington, DC: US Govt Printing Office)
Peterkop R K and Liepinysh A K 1979 *Proc. Latv. Acad. Sci.* **2** 3 (in Russian)
Shafranyosh I I and Margitich M O 1996 *Z. Phys.* D **37** 97–101
Shafranyosh I I, Snegurskaya T A and Aleksakhin I S 1990 *Opt. Spektrosk.* **68** 262 (in Russian)
—— 1994a *Opt. Spectrosc.* **76** 20
Shafranyosh I I, Snegurskaya T A and Margitich M O 1994b *Opt. Spektrosk.* **77** 725 (in Russian)
Striganov A R and Sventitsky N C 1996 *Tables of Spectral Lines of Neutral and Ionized Atoms* (Moscow: Atomizdat)
Stumpf B and Gallagher A C 1985 *Phys. Rev.* A **32** 3344
Trajmar S and Nickel J C 1993 *Adv. At. Mol. Opt. Phys.* **30** 45
Vaeck N, Godefroid M and Hansen J E 1991 *J. Phys. B: At. Mol. Opt. Phys.* **24** 361
Vainshtein L A, Sobelman I I and Yukov E A 1979 *Excitation of Atoms and Broadening of Spectral Lines* (Moscow: Nauka) (in Russian)
Van Zyl, Dunn G H and Chamberlain G 1980 *Phys. Rev.* A **22** 1916
Zatsarinny O I, Lengyel V I and Masalovich E A 1989 *Opt. Spectrosc.* **67** 20
—— 1991 *Phys. Rev.* A **44** 7343